



Implementation of the Wobbling Technique with Spatial Resolution Enhancement Approach in the Xtrim-PET Preclinical Scanner: Monte Carlo Simulation and Performance Evaluation

Bahador Bahadorzadeh^{1,2}, Reza Faghihi^{1,3*} , Ahdiyeh Aghaz⁴, Sedigheh Sina^{1,3}, Arman Rahmim⁵, Mohammad Reza Ay^{2,6*} 

¹ Nuclear Engineering Department, School of Mechanical Engineering, Faculty of Engineering, Shiraz University, Shiraz, Iran

² Research Center for Molecular and Cellular Imaging, Advanced Medical Technologies and Equipment Institute, Tehran University of Medical Sciences, Tehran, Iran

³ Radiation Research Center, Shiraz University, Shiraz, Iran

⁴ Radiation Application Research School, Nuclear Science and Technology Research Institute, Tehran, Iran

⁵ Departments of Radiology and Physics Vancouver, The University of British Columbia, Vancouver, Canada

⁶ Department of Medical Physics and Biomedical Engineering, School of Medicine, Tehran University of Medical Sciences, Tehran, Iran

*Corresponding Authors: Reza Faghihi, Mohammad Reza Ay
Email: Faghihir@Shirazu.ac.ir, Mohammadreza_ay@tums.ac.ir

Received: 24 September 2023 / Accepted: 02 December 2023

Abstract

Purpose: This study aims to develop and implement a wobbling data acquisition mode in the Xtrim-PET scanner to enhance spatial resolution in preclinical Positron Emission Tomography (PET) imaging.

Materials and Methods: To evaluate the performance of the Xtrim-PET scanner with the wobbling motion, simulations were conducted using the Gate Monte Carlo toolkit. The positions of all detected Lines Of Responses (LORs) were adjusted based on the magnitude of the wobbling movement to minimize image blurring. Different stop point configurations ranging from 4 to 256 were investigated to optimize the number of wobbling points. The performance of the wobbling data acquisition mode was assessed using IQ NEMA-NU4 and Hot-Rod phantoms, as well as phantoms resembling mice and rats. Two reconstruction methods were employed to assess image quality: Filtered Back-Projection (FBP) with various filters and the iterative method, OSEM, with 5 and 10 iterations.

Results: The results from NEMA tests using Monte Carlo simulations closely matched experimental measurements, demonstrating the accuracy of the simulations. Based on sinograms obtained from the uniform cylinder phantom scan and considering the constraints associated with the mechanical movement system, it was decided to use 4 stopping points for the wobbling movement. The implementation of the wobbling technique resulted in a spatial resolution of 0.91 mm at the center of the scanner, while without the technique, the resolution was 1.93 mm. The wobbling motion did not significantly affect sensitivity, NECR, or SF values. However, it notably improved spatial resolution, especially with the OSEM method, enhancing image quality by up to 52.8%.

Conclusion: The wobbling technique offers a substantial enhancement in spatial resolution for preclinical PET scanners. Although achieving sub-micrometer spatial resolutions theoretically seems feasible by increasing the number of stopping points, practical limitations present challenges. Nonetheless, the wobbling technique shows promise, providing an approximate 50% improvement in spatial resolution.

Keywords: Positron Emission Tomography; Preclinical Scanner; Gantry Wobbling; Monte Carlo Simulation.

1. Introduction

Nuclear medicine has become a prominent field in cancer diagnosis and treatment due to the advancements in radiation engineering science. It is widely recognized as one of the most utilized medical sciences in this domain. Positron Emission Tomography (PET) imaging device is employed to administer radiopharmaceuticals for timely diagnosis, particularly in the early stages of diseases [1, 2]. These nuclear medicine techniques offer valuable insights into metabolic processes and organ functions by providing detailed image information [3-6].

PET scanners face challenges in optimizing the detector size, sensitivity, and sampling size, which involve a trade-off between spatial resolution and scanner sensitivity. The demand for high-resolution imaging, particularly in brain imaging, has significantly increased in the development of new clinical PET systems. To address the limitations of PET spatial resolution, the wobbling technique has been proposed and utilized [7]. In 2016, Hang-Keun Kim and colleagues performed a study aiming to implement wobbling and employ the LSF-based MLEM image reconstruction method in PET with wobbling. They evaluated a new MLEM algorithm, WL-MLEM, based on LSF for PET with wobbling, without reducing the detector crystal size. Through simulations, they compared its performance with existing algorithms, including conventional MLEM and LSF-based MLEM. The simulation results demonstrated that the WL-MLEM algorithm achieved superior spatial resolution and image quality compared to PET systems without wobbling, using conventional algorithms [8].

In 2019, Zang-Hee Cho and colleagues performed a study focusing on the development of wobbling and zoom PET for molecular imaging, aiming to achieve high resolution and sensitivity. The study proposed a convertible PET system capable of switching between brain and body imaging modes, incorporating wobbling and zooming features. The results revealed that the proposed system achieved a spatial resolution of up to 1.56 mm in Full Width at Half Maximum (FWHM) in a brain imaging mode. In both phantom brain imaging and in vivo studies of rat brains, the proposed system exhibited superior image quality when compared to conventional PET systems [9].

In 2019, Sheikhzadeh and colleagues performed a comprehensive study where they accurately modeled

Xtrim-PET using the GATE framework. Their work extended beyond modeling, as they proceeded to design and optimize the BM-PET scanner based on this model. To enhance the simulated data, the researchers developed resolution recovery and attenuation correction techniques, which were successfully implemented. The optimized BM-PET system, featuring a rotating cylindrical geometry and LYSO-SiPM detectors, exhibited a notable system sensitivity of approximately 16 cps/kBq and achieved a spatial resolution of 2.1 mm FWHM according to the NEMA standard. This achievement can be attributed to the optimization of the BM-PET geometry and detector configuration, the introduction of scanner rotation/wobbling, and the utilization of image correction and enhancement techniques. These advancements in performance have paved the way for the production of a prototype scanner, demonstrating the potential of the modeled brain PET system [10].

Among the limited research performed in Iran within this field, Emami *et al.* carried out a study in 2020 to evaluate the performance of a dedicated breast PET scanner and enhance its spatial resolution using wobbling, employing Monte Carlo simulations. Preliminary simulation studies were performed to predict various parameters for the new design, including spatial resolution, absolute sensitivity, Noise Equivalent Count Rate (NECR), and Scattering Fraction (SF). The findings indicated that the absolute sensitivity of their design reached 1.42%, surpassing that of other commercial breast PET systems. Additionally, SF and NECR were calculated as 20.6% and 21.8 kcps, respectively [11].

PET scanners have recently gained attention from researchers for pre-clinical testing and studying the distribution of radiopharmaceuticals in healthy or diseased tissues of small laboratory animals [12, 13]. However, ensuring the accuracy of these tests in pre-clinical laboratories necessitates qualitative and quantitative evaluation of high-resolution images. Currently, no studies have been performed in the country on the performance of preclinical PET scanners using a wobbling gantry approach to enhance spatial resolution. This study aims to develop and implement a wobbling data acquisition mode in the Xtrim preclinical PET scanner with the objective of enhancing spatial resolution in molecular imaging.

2. Materials and Methods

2.1. Monte Carlo Simulation

Monte Carlo simulation is a fundamental tool utilized in tomography imaging to aid in the design of new medical imaging devices, assess and implement novel image reconstruction algorithms, and scatter correction techniques, and optimize scan protocols. In this study, Gate v8.0 software, a versatile program based on the GEANT4 Monte Carlo code, was employed to simulate and evaluate the performance of the Xtrim-PET scanner.

The input code in Gate software for modeling the Xtrim-PET scanner comprised several steps. First, the scanner geometry was defined, followed by the definition of the phantom geometry. Next, the interaction physics processes were set, and the simulation was initialized. Subsequently, the detector modeling, radioactive source definition, output data format determination, and data acquisition in the simulation were established.

Various interactions were considered and detected in the simulation, including the photoelectric effect, Compton scattering, Rayleigh scattering, multiple scattering, pair production, ionization, bremsstrahlung production, positron annihilation, annihilation photon misalignment, and radioactive decay. To enhance output accuracy and ensure reasonable execution time, variance reduction and cutting techniques were implemented in the simulation. To prevent divergence in the simulation calculations, a threshold was defined for charged particle interactions with the environment. This threshold was set as a distance of 1 mm or an energy cutoff for each specific material, ensuring accurate and efficient simulation results.

The output data from the scanner simulation is recorded in ASCII format, capturing 46 characteristics for each coincidence event involving two photons, or 23 characteristics for each individual coincidence photon. The term "ASCII" refers to the raw simulation output file that contains essential information such as IDs of the run, event and source, XYZ position of the source, time, energy, XYZ position of interaction, volume IDs, and number of Compton and Rayleigh interactions, all saved in the ASCII format. To facilitate further analysis, the raw

output file from the simulation was converted into the standard List-Mode format. To accomplish this objective, the main characteristics of each coincidence event were extracted from the ASCII output and organized according to the output standard in list-mode format. The resulting data was then stored in the standardized LMF format.

To reduce the duration time of the simulation, the tracking of light photons produced in the crystal and the determination of the interaction position using the weight fraction of light detected by SiPM were excluded. Instead, the interaction location of the coincidence photons was directly obtained from the raw output of the simulator. This approach was chosen to expedite the simulation process.

The programming was performed using MATLAB 2019 software, which allowed for the utilization of the simulation output file saved in the List-Mode Format (LMF) as input. All the parameters in the LMF file were categorized and stored in separate matrices.

For the reconstruction of 2D images from the 3D sinogram matrix, the Rebinning process (SSRB) was initially applied to the output data. In order to execute SSRB rebinning, a MATLAB program that corrects the Z values (axial direction) of the Lines Of Response (LORs), was developed. This process facilitated the formation of 2D sinograms corresponding to each slice along the axial direction. Subsequently, MATLAB software was employed to perform corrections on the sinogram matrix obtained from the simulation. These corrections encompass attenuation, efficiency, and geometric adjustments, ensuring accurate image reconstruction.

In essence, the two dimensions of the 3D sinogram matrix correspond to the radial distance (r) and the data acquisition angle (φ) in the transverse plane. The radial distance represents the interaction position along the detector, while the data acquisition angle signifies the angular position from which the data was acquired.

Generally, to obtain the 2D sinogram, the positions (x, y, z) of coincidence photon interactions with the crystal were used to generate the Lines Of Response (LORs). Following that, the SSRB rebinning process was performed. Subsequently, for each specific slice corresponding to a two-dimensional plane, the LORs were assigned r and φ values based on their distances

from the center and slopes, respectively. By utilizing these assigned values, 2D sinograms were subsequently generated.

2.2. Xtrim-PET Scanner

The Xtrim-PET scanner, developed by Perto Negar Persia Company, is a specialized instrument for pre-clinical PET tomography imaging of small animals. This scanner is equipped with 10 detector blocks, with each block comprising a grid of 24×24 LYSO crystals connected to SiPM photodiodes (Figure 1).

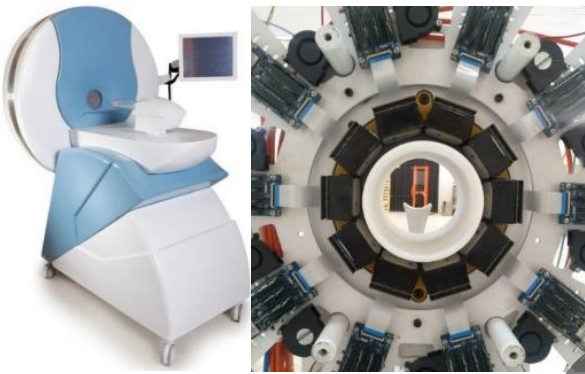


Figure 1. The Xtrim-PET scanner and arrangement of blocks

Based on the technical documentation supplied by the manufacturer of the Xtrim-PET scanner, comprehensive simulations were performed to evaluate all the key components of the scanner. The dimensions and materials of each component were meticulously considered during the simulation process [14] (Table 1).

Table 1. Xtrim-PET scanner specific details [14]

Specification	Value
Crystal size	$2 \times 2 \times 10$ mm
Crystal material	LYSO
Number of blocks	10
Number of crystals in each block	24×24
Number of detector rings	24
Axial FOV	50 mm
Transaxial FOV	100 mm
Coincidence window	5 ns
Energy window	250-650 keV

2.3. NEMA Phantoms and Image Quality

To assess the performance and image quality of the simulated scanner, the Image Quality (IQ) phantom was employed, following the guidelines outlined in the NEMA Standards NU4-2008. Initially, the IQ phantom was simulated, featuring an external diameter of 33.5 mm and a height of 56 mm. This phantom includes tubular holes with diameters of 1, 2, 3, 4, and 5 mm, as well as a uniform section with a diameter of 30 mm. Additionally, it consists of two holes filled with air and water, each with a diameter of 8 mm and a height of 15 mm

For both quantitative and qualitative evaluations of scanner resolution, the Hot-Rod phantom with standard dimensions was simulated and utilized. The QRM-MicroPET-HotRod phantom comprises a cylindrical structure made of PMMA, with an outer diameter of 35 mm and a height of 70 mm. It contains a series of rod-shaped holes with diameters of 0.6, 0.8, 1.0, 1.2, 1.5, and 2.0 mm, enabling the evaluation of spatial resolution characteristics.

In addition, simulations of mouse and rat phantoms were performed to assess the coincidence count rates and SFs. The mouse phantom is designed as a circular cylinder with dimensions of 70 mm in length and 25 mm in diameter, constructed from polyethylene material. Within this phantom, there is a cylindrical hole with a diameter of 3.2 mm, positioned parallel to the central axis at a radial distance of 10 mm. This hole serves as a channel for introducing the radioactive solution.

Similarly, the Rat phantom exhibits a similar geometry but with larger dimensions. It consists of a cylinder measuring 50 mm in diameter and 150 mm in length. Like the mouse phantom, it contains a cylindrical hole with a diameter of 3.2 mm, positioned parallel to the central axis, but at a greater radial distance of 17.5 mm.

2.4. Validation Strategy

The validation of the simulation model was performed by comparing the key parameters of the scanner, such as sensitivity, the coincidence count rate, NECR (noise equivalent count rate), and SF. These parameters were obtained from the simulation,

and their values were compared to the measurements obtained from the actual scanner.

2.5. Data Acquisition with Wobbling Motion

Following the simulation of the scanner and validation, the wobbling motion design was implemented on the gantry during the data acquisition process. The implementation of gantry wobbling motion in the simulation involved the utilization of the Generic move, along with the preparation of the placements file. The placements file contains the transformations (rotation, translation) and the time value where this transformation was applied. Both with and without gantry wobbling, the data acquisition was carried out in the simulation. The acquired data was then saved in the LMF format, and subsequent image reconstruction was performed using NiftyRec software developed by the Medical Image Computing Center at University College London, England [15]. Finally, the performance evaluation of the scanner, along with quantitative and qualitative analysis of the reconstructed images, was performed.

To enhance sampling in the transverse plane, as well as the axial and tangential directions, and eliminate sinogram gaps caused by the spacing between detector blocks within each ring, as well as inactive distances between crystals within each block, a wobbling motion of the gantry was employed in the simulation (Figure 2).

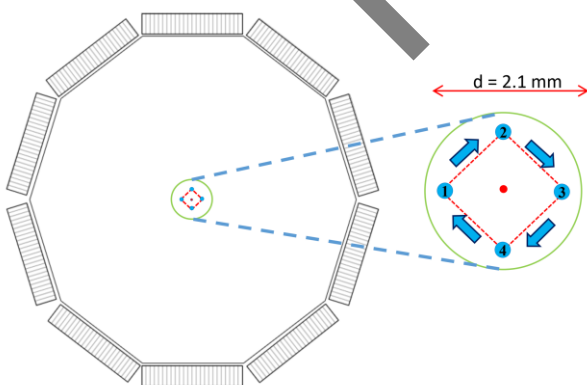


Figure 2. A schematic representation of the gantry wobbling motion with a 1.05 mm radius at its center, and data acquisition taking place at four different positions with designated stopping points

To enhance comprehension of Figure 2, a minimum of 4 stop points were considered during its creation. This motion involved rotating the gantry in a circular

motion around the center of the gantry using a radius equal to the crystal pitch (the distance between the centers of two adjacent crystals) or the crystal width (1.2 mm).

To implement this, the entire scan duration was divided into four segments, and in each segment, the gantry's center was positioned in one of the locations depicted in Figure 3. Subsequently, upon completion of the imaging process, the r and ϕ coordinate values associated with each Line Of Response (LOR) in the 3D sinogram were adjusted relative to the reference position where the gantry was in the center position.

In essence, the sinograms from all four sections were adjusted based on the displacement of the gantry center. Subsequently, these corrected sinograms were combined, resulting in the formation of the final sinogram, which was then reconstructed.

To optimize the number of stopping points and assess the effectiveness of sinogram gap elimination through gantry wobbling, various stopping points were employed in the scanner simulation, including 4, 8, 16, 32, 64, 128, and 256. Data acquisition was performed using a uniform active phantom (Radioisotope F-18) in the form of a cylinder with a diameter equivalent to the Field Of View (FOV).

Furthermore, in order to evaluate spatial resolution according to the NEMA standard, 4-point sources (F-18) were incorporated into the simulation at radial distances of 5, 10, 15, and 25 mm. Data acquisition was carried out in two modes, with and without gantry wobbling motion.

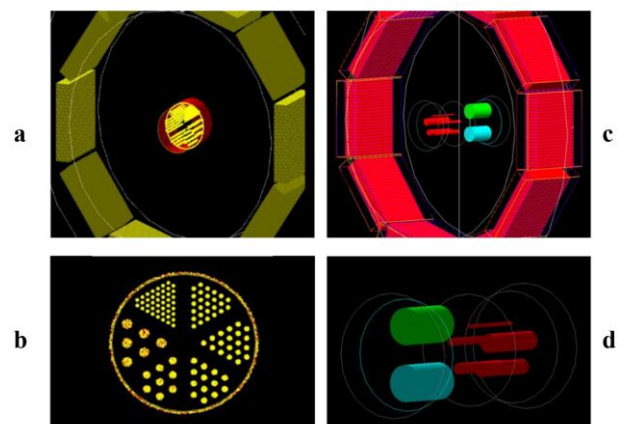


Figure 3. Simulated Xtrim-PET scanner geometry with a) Hot-Rod phantom and c) NEMA-NU4 phantom and, also b) QRM-HotRod phantom and d) NEMA-NU4 phantom geometry (right side)

2.6. Performance Evaluation: With and Without Wobbling

Following the implementation of the wobbling motion and subsequent image reconstruction, the reconstructed images were utilized for the assessment of image quality. Quantitative parameters related to image quality were compared using MATLAB software, AMIDE version 4.0.1 (a medical imaging data tester), and ImageJ (version i1.50, National Institutes of Health, USA).

To evaluate image quality, the IQ image quality phantom was employed. This phantom facilitated the examination of hot lesions, uniform hot areas (containing active solution), and cold areas (containing inactive solution and air) with specific activity concentrations.

The reconstructed images from the scanning procedure were subject to the necessary corrections. Subsequently, using software, the maximum, minimum, and average values of uniformity, along with their corresponding standard deviations, were calculated within the defined Regions Of Interest (ROIs).

To determine the Recovery Coefficients (RC) and their standard deviations, the maximum pixel value within each ROI and the corresponding profile were utilized. These calculations were performed for holes with diameters ranging from 1 mm to 5 mm. The RC values were obtained by comparing the pixel values to the uniformity value derived from the uniformity section of the phantom.

Lastly, the SOR (Spill-over Ratio) values were computed by measuring the ratio of the average pixel values in the cold areas (containing inactive solution and air) to the average value of uniformity.

Additionally, the Hot-Rod phantom was employed to assess the spatial resolution of the scanner qualitatively. This phantom consists of cylindrical compartments with diameters ranging from 0.6 mm to 2.0 mm, designed for the placement of the active solution (Figure 3b).

The reconstructed images obtained from both data acquisition modes underwent evaluation using both Filtered Back-Projection (FBP) and iterative methods. Initially, image reconstruction from the 2D sinogram was performed using the back-projection method,

employing filters such as Ram-Lak, Shepp-logan, Cosine, Hamming, and Hann. Subsequently, the image was reconstructed using the iterative method of OSEM (Ordered Subsets Expectation Maximization), utilizing 5 iterations and 4 subsets, through the use of NiftyRec software.

3. Results

3.1. MC Simulations: Geometry and Phantoms

The scanner simulation was performed, employing a geometry based on the dimensions and design drawings of the physical scanner (Figure 3a and 3c). Additionally, to qualitatively assess the spatial resolution of the reconstructed image, simulation was performed for the IQ NEMA-NU4 and QRM-MicroPET Hot-Rod image quality evaluation phantoms used in this study. These phantoms were simulated to match their respective dimensions and components (Figure 3b and 3d).

3.2. Validation

The results obtained from the NEMA tests, comprising both Monte Carlo simulations and experimental measurements, are presented below. The tests include spatial resolution, sensitivity, NECR, and SF.

Spatial resolution: At a radial distance of 5 mm from the Center of the Field Of View (CFOV), the radial FWHM values were 1.93 mm and 1.95 mm for the Monte Carlo simulation and experimental measurement, respectively. Similarly, the tangential FWHM values were 1.92 mm and 1.94 mm, respectively. When considering different radial distances, the maximum difference between the spatial resolution values obtained from the simulation and measurement was found to be 12%.

Sensitivity: The absolute peak sensitivity, simulated using a time window of 5 ns and an energy window of 250-650 keV, was determined as 3.14%, while the measured sensitivity was slightly lower at 3.02%. It is noteworthy that the simulated sensitivities at all axial positions were approximately 4 to 6% higher than the measured sensitivities.

NECR and SF: For the mouse phantom with an activity concentration of 0.36 MBq/cc, the peak NECRs obtained from the simulated and measured data were 118.7 kcps and 115.3 kcps, respectively. Similarly, for the rat phantom with an activity concentration of 1.50 kBq/cc, the simulated and measured peak NECRs were found to be 86.7 kcps and 83.8 kcps, respectively. The SFs were also evaluated, resulting in simulated values of 12.2% and 25.1% for the mouse and rat phantoms, respectively, while the measured SFs for the corresponding phantoms were 13.1% and 27.5%. Comparing the simulated model with the measured results, differences of 7% and 9% were observed for NECR and SF, respectively.

The close agreement observed between the Monte Carlo simulation and experimental measurement confirms the accuracy and reliability of the simulation results. This comparison validates the effectiveness of the simulation approach.

3.3. Data Acquisition with Wobbling Motion

In order to optimize the number of stop points in the gantry wobbling motion and assess the reduction of gaps in the sinogram, a uniform cylindrical phantom was utilized for data acquisition. The stop points were set at 4, 8, 16, 32, 64, 128, and 256. A simulated scanner was employed to form the sinogram (Figure 4).

In the wobbling gantry design, the coincidence detection system intentionally avoids recording any coincidences while the gantry is transitioning between two stop points, aiming to prevent artifacts. Consequently, as the number of stop points increases during the fixed scan period, the inactive time of the coincidence detection system also increases, leading to a decrease in the number of detected coincidences compared to the data acquisition mode without wobbling motion. The impact of this decrease in coincidence detection is minimal when the number of stop points is small, as the time spent on the wobbling motion is relatively small to the total scan time. However, as the number of stop points increases to 128 and 256, the time dedicated to the wobbling motion becomes a significant portion, resulting in a more noticeable reduction in the number of detected coincidences in the sinogram.

The sinograms displayed in Figure 4 demonstrate that as the number of stop points increases, the gaps in the sinogram are compensated for and eventually disappear. Moreover, beyond 16 stop points, no noticeable difference was observed in terms of gap disappearance and sinogram uniformity.

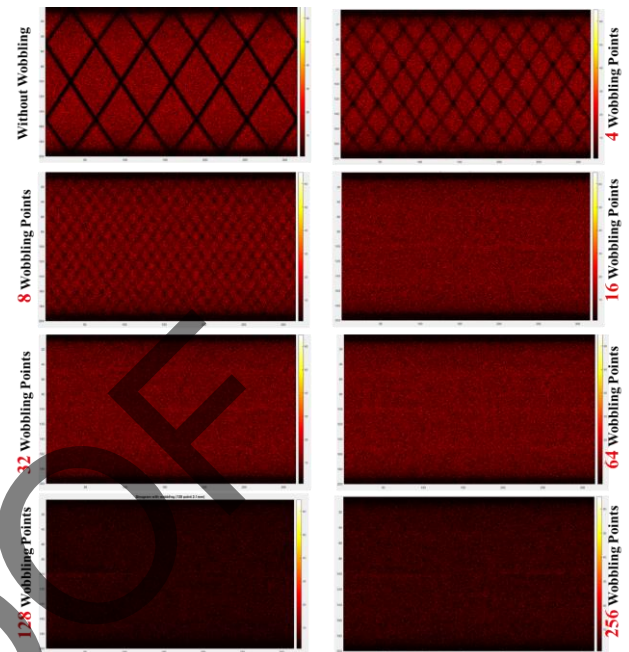


Figure 4. Sinograms obtained from a uniform cylindrical source (F-18) by the gantry wobbling data acquisition mode with a different number of stop points (sinogram size: 200×315 and pixel size: 0.5 mm)

3.4. Performance Evaluation: With and Without Wobbling Motion

The key parameters of the preclinical Xtrim-PET scanner were assessed using the NEMA NU4 standard methods for two data acquisition modes: one with wobbling motion and the other without. The sensitivity, NECR, and SF values were calculated for both modes, and the results matched those reported in Section 3.2. Based on these results, it can be concluded that the wobbling motion has no significant impact on the sensitivity, NECR, and SF parameters.

Table 2 presents the spatial resolution results of the scanner in the radial, tangential, and axial directions. These spatial resolution values were evaluated for four radioactive point sources at radial distances of 5, 10, 15, and 25 mm in the simulation, considering both data acquisition modes without (Figure 5a) and with wobbling motion (Figure 5b).

The sinogram (Figure 6a) gaps in the wobbling mode, for the case of four-point sources within a 10 cm FOV, exhibit significantly reduced gaps, leading to a more uniform sinogram. The evaluation of spatial resolution for both data acquisition modes, with and without wobbling motion, was performed using the OSEM iterative method with 10 iterations and 4 subsets (Figure 6b and c).

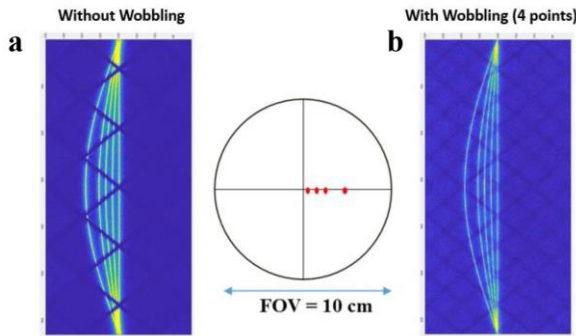


Figure 5. Sinograms obtained from 4-point sources, at radial distances of 5, 10, 15, and 25 mm from the center in two modes a) without and, b) with wobbling motion

Upon examining the FWHM values obtained from the data acquisition modes involving wobbling motion, it is evident that the spatial resolution improves. This indicates that increasing the number of samples results in decreased spatial resolution, leading to enhanced image quality.

Table 2. Simulated spatial resolutions (FWHM) at the axial center according to NEMA NU4 standard

Reconstructed image pixel size (mm): 0.33 Slice Thickness (mm): 0.26				
With wobbling				
	5 mm	10 mm	15 mm	25 mm
	FWHM*	FWHM	FWHM	FWHM
Radial	0.91	0.99	1.13	1.29
Tangential	0.90	1.00	1.11	1.28
Axial	1.89	2.05	2.15	2.31
Without wobbling				
Radial	1.93	2.21	2.30	2.46
Tangential	1.92	2.23	2.31	2.45
Axial	1.90	2.13	2.28	2.41

*FWHM: Full width at half maximum

It was observed that the implementation of gantry wobbling motion with 4-stop points, using the OSEM iteration reconstruction method, can improve spatial

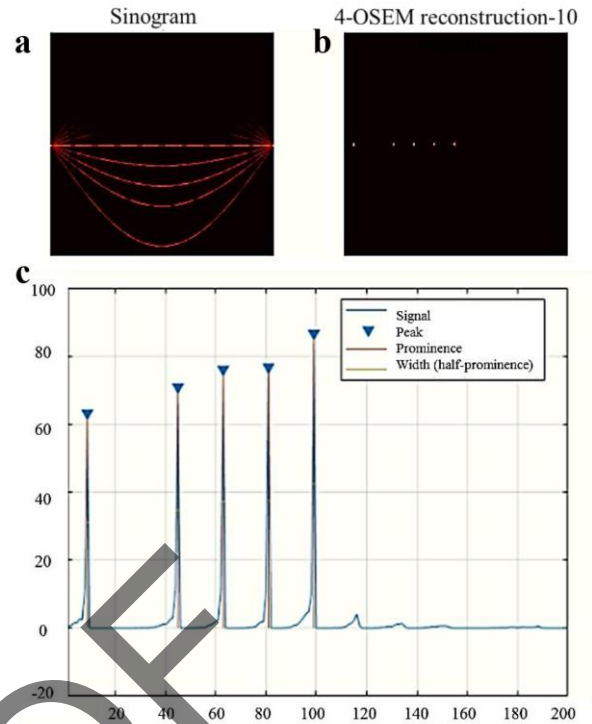


Figure 6. a) Sinogram, b) reconstructing the image of point sources by OSEM iterative method, and c) PSF linear profile

resolution by up to 52.8%. This improvement is attributed to the reduction in sampling size achieved through the wobbling technique.

3.5. Analysis of Wobbling Mode Images

The reconstructed images obtained from both data acquisition modes were evaluated and compared with back-projection filter methods and iterative methods. Initially, image reconstruction from 2D sinograms was performed using the back-projection method, employing Ram-lak, Shepp-logan, Cosine, Hamming, and Hann filters for the data acquisition modes without wobbling motion (Figure 7a) and with wobbling motion (Figure 7b).

Subsequently, the image reconstruction process continued with the use of the OSEM (Ordered Subset Expectation Maximization) method. In this approach, sinograms acquired from the Hot-Rod image quality phantom scan were reconstructed with 5 and 10 iterations and 4 subsets, covering FOVs (Figure 8b and c).

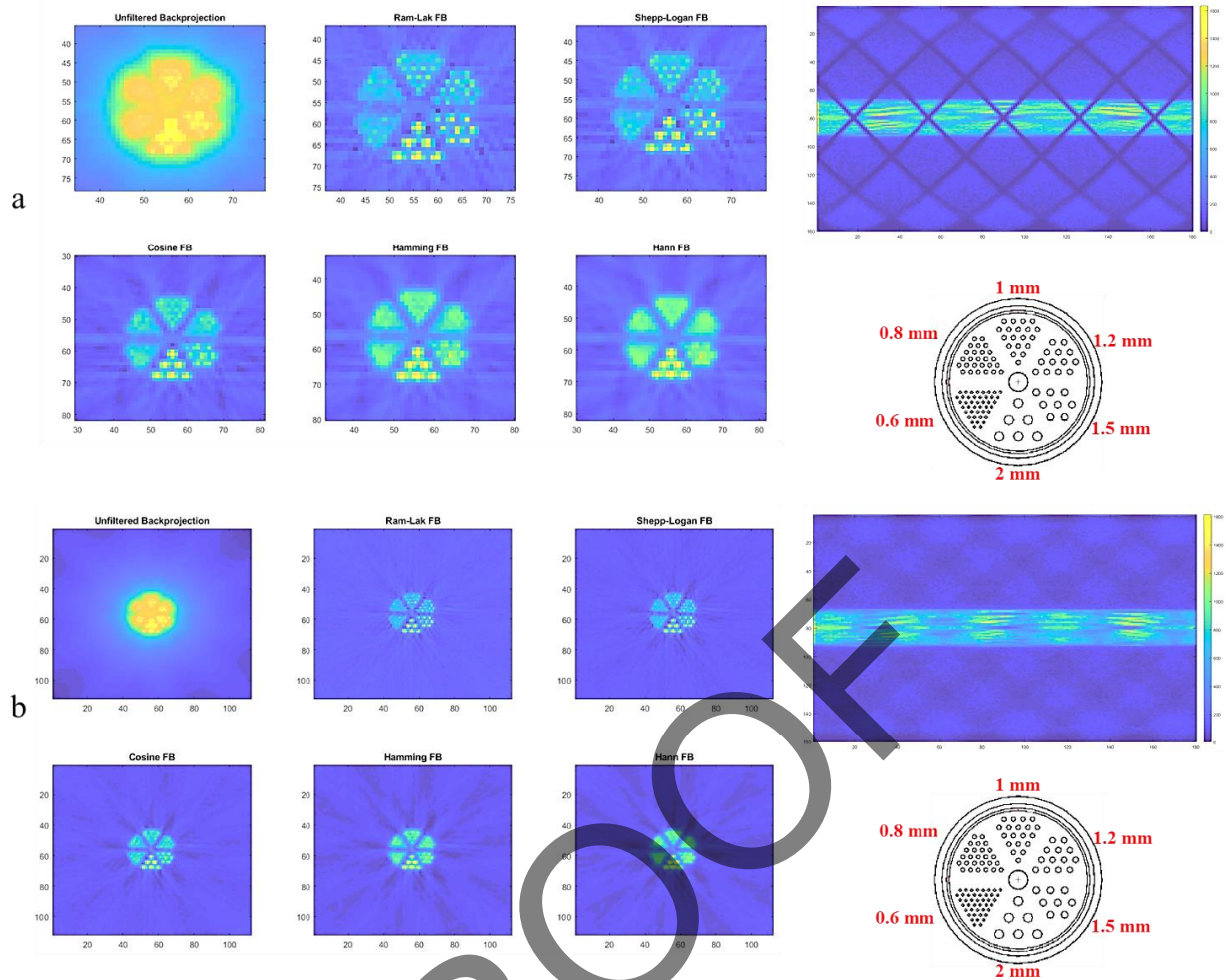


Figure 7. Reconstructed images by back-projection filter method obtained from Hot-Rod phantom scan with data acquisition mode a) without wobbling and b) with wobbling motion

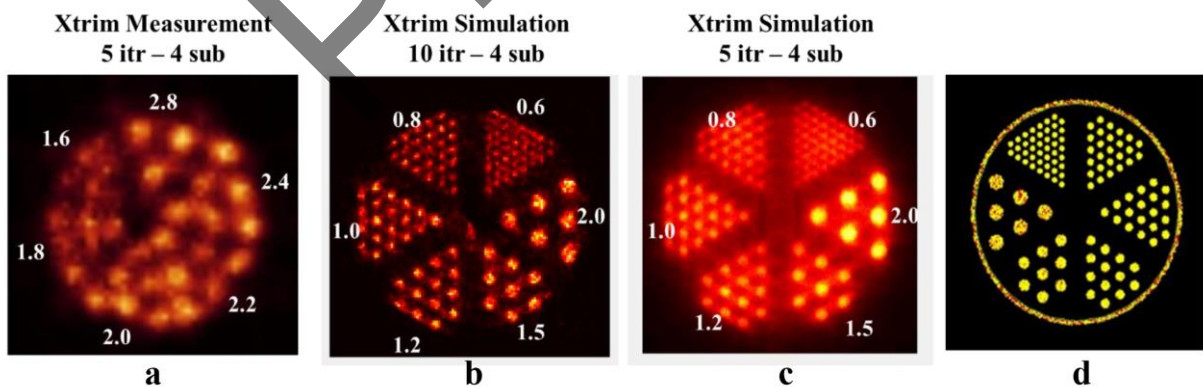


Figure 8. Comparison between reconstructed images by OSEM iteration method obtained from a) measurement without wobbling utilized 5 iterations and 4 subsets, b) simulation wobbling utilized 10 iterations and 4 subsets, c) simulation wobbling utilized 5 iterations and 4 subsets, and d) simulation of Hot-Rod phantom

As depicted in [Figure 8](#), the spatial resolution of the image obtained from the actual scanner ([Figure 8a](#)) is qualitatively estimated to be approximately 2 mm. Conversely, in the reconstructed images obtained by

simulating the data acquisition mode with wobbling motion, the qualitative spatial resolution for 5 and 10 iterations ([Figure 8b](#) and [c](#)) is estimated to be around 1.0 mm and 0.8 mm, respectively. Additionally, upon

evaluating the image reconstruction methods of FBP and OSEM, it can be inferred that the OSEM method exhibits superior performance in terms of spatial resolution.

4. Discussion

The utilization of gantry wobbling data acquisition mode in preclinical PET scanners offers the potential to enhance system performance and accuracy, thereby enabling the generation of high-resolution images for research purposes. In addition, this data acquisition mode holds the promise of producing cost-effective scanners, provided that the design and calculation of the device's output factors are optimized accordingly.

Figure 4 illustrates that an increase in the number of stop points up to 16 during the gantry wobbling motion results in enhanced sampling in the transverse plane and compensates for and eliminates gaps in the sinogram. However, surpassing this threshold does not yield a noticeable difference in the sinogram. Therefore, based on considerations such as crystal dimensions, block size, and the diameter of the central circle where the wobbling motion occurs, it can be concluded that, for the Xtrim-PET scanner, 16 stop points are sufficient during imaging to achieve increased sampling intervals and eliminate sinogram gaps. Further increasing the number of stop points does not provide additional benefits to the scanner output. However, practical considerations impose limitations on the implementation of a large number of stopping points. As a result, in this study, a conservative approach was taken, and a total of 4 stopping points were used to concurrently increase sampling and eliminate gaps in the data acquisition process.

Based on the findings presented in Table 2, the implementation of gantry wobbling motion in the Xtrim-PET scanner leads to an average of 50% reduction in radial, tangential, and axial resolution, thereby enhancing the image quality. However, it is important to note that an artifact can arise in the reconstructed images due to an excessive number of sampling intervals resulting from increased sampling in the transverse plane and an increased number of sinogram matrix intervals.

Figure 7 demonstrates that the data acquisition mode with wobbling motion exhibits an increased spatial resolution compared to the mode without wobbling

motion. Furthermore, the application of different filters does not yield a significant difference in both data acquisition modes. The gantry wobbling motion effectively compensates for gaps in the sinogram, resulting in reconstructed images that display greater consistency compared to the mode without wobbling motion.

The reconstructed images presented in Figure 8 (b and c) reveal that, within a sinogram matrix of fixed dimensions and detected coincidences, the spatial resolution is more favorable in smaller FOV settings. Additionally, in terms of quality, the observed spatial resolution in this particular image reconstruction is approximately 0.8 mm, representing a notable 60% improvement in spatial resolution compared to the data acquisition mode without wobbling motion.

In comparison to previous studies, our findings on the Xtrim-PET preclinical scanner utilizing the gantry wobbling method align with and, in some instances, surpass the results reported in other research articles.

Thompson *et al.* (2005) reported their efforts in improving the spatial resolution of the microPET scanner using the bed wobbling technique. Their research predominantly emphasized technological implementation and did not delve deeply into the quantitative improvements of the resolution. While they presented a groundwork for utilizing wobbling, our study enhanced upon this premise by offering a detailed quantitative analysis of resolution improvement and provided an optimized approach to the number of stop points.

Suk *et al.* (2008) further built upon the foundation laid by Thompson, specifically for the MicroPET R4 scanner. They reported improvements in spatial resolution using the bed wobbling technique but did not engage extensively with varying stopping points. Our study differs in this regard, as we examined the impact of varying stop points in depth, identifying an optimal number (16 stop points) that offers maximal benefits.

Cho *et al.* (2019) introduced a novel concept of "wobbling and zooming" to enhance both sensitivity and resolution in molecular imaging. While their study focused on a unique combination of methods, they reported substantial improvements in spatial resolution using the wobbling technique. Our findings are in line with theirs, especially in terms of percentage improvement. Additionally, the idea of "zooming" could

be a future direction to further improve the capabilities of the Xtrim-PET scanner.

Emami *et al.* (2020) targeted breast PET imaging and explored the potential advantages of using the wobbling method to enhance spatial resolution. Their Monte Carlo simulation results exhibited improved spatial resolutions with wobbling, similar to the findings from our study. The significance of their work lies in the application to a specific clinical context (breast imaging), highlighting the adaptability and versatility of the wobbling technique.

The consistency in findings across these studies, including ours, emphasizes the efficacy and reliability of the wobbling technique in PET scanners, especially in improving spatial resolution. Notably, our study contributes an in-depth analysis of the relationship between the number of stopping points during the gantry wobbling motion and the resultant spatial resolution. This facet was not thoroughly examined in the previously referenced studies, adding a novel dimension to the growing body of literature on this subject. Furthermore, our research builds on the potential benefits of gantry wobbling not just in terms of improved resolution, but also from a cost-effectiveness standpoint. The potential to design and produce high-resolution scanners without exponentially increasing costs offers promising implications for the broader accessibility of advanced imaging tools in research and clinical settings. In conclusion, while the referenced articles collectively illustrate the potential of the wobbling technique in enhancing PET scanner capabilities, our study offers a detailed, optimized approach for its implementation, yielding significant improvements in spatial resolution and presenting opportunities for cost-effective scanner designs.

Although the wobbling motion data acquisition mode leads to an increased sampling rate in the transverse plane, resulting in improved radial and tangential resolution, there is no change in the resolution along the axial direction. The Xtrim-PET scanner, when utilizing the wobbling data acquisition mode, exhibits a radial resolution of 0.91 mm and a tangential resolution of 0.90 mm. These values indicate superior and comparable resolution compared to other resolutions observed in preclinical PET systems. These spatial resolution values are comparable to those reported for other preclinical PET systems such as Micro-PET R4 (2.13 mm, FORE+FBP) [16], Argus (1.63 mm, 2D FBP) [17],

microPET Focus-120 (1.92 mm, FORE+FBP) [18], VrPET (1.52 mm, SSRB+FBP) [19], LabPET8 (1.65 mm, SSRB+FBP) [20], Albira Iring (1.65 mm, SSRB+FBP) [21], TransPET-LH (0.95 mm, 3D OSEM) [22], and SAFIR (2.6 mm, FBP3DRP) [23] that possess approximately radial resolution at 5mm distance from center of TFOV.

It should be noted that the results presented in this study were obtained from Monte Carlo simulations, and thus, the actual implementation of gantry wobbling movement may introduce errors in the mechanical motion of the gantry and the positioning of the gantry center at the stop points. The uncertainty associated with these errors and their repeatability should be quantified. Consequently, it is expected that the actual improvement in spatial resolution during practical measurements will be lower than what is demonstrated in the simulation presented in this research. The mechanical design function and the corrections applied in data acquisition should be taken into consideration when implementing the wobbling motion data acquisition mode to determine the actual extent of spatial resolution improvement.

5. Conclusion

Through simulation calculations and theoretical analysis, it is theoretically possible to achieve spatial resolution values of less than micrometers by increasing the number of stopping points and the sampling intervals. However, in practical terms, such a substantial reduction in spatial resolution is not feasible in real scanners due to constraints related to coincidence detected efficiency, motion mechanics, and scanner electronics. Nevertheless, the results indicate that the implementation of wobbling motion during imaging can lead to an improvement in spatial resolution of approximately 50%.

Acknowledgments

The authors would like to extend their gratitude to Parto Nagar Persia Company for their provision of the essential equipment and systems. This work is supported by grant number 41652 Tehran University of Medical Sciences.

References

- 1- Gerd Muehlehner and Joel S Karp, "Positron emission tomography." *Physics in Medicine & Biology*, Vol. 51 (No. 13), p. R117, (2006).
- 2- Nic Gillings, "Radiotracers for positron emission tomography imaging." *Magnetic Resonance Materials in Physics, Biology and Medicine*, Vol. 26pp. 149-58, (2013).
- 3- Habib Zaidi, Quantitative analysis in nuclear medicine imaging. *Springer*, (2006).
- 4- Kiran Kumar Solingapuram Sai, Zuzana Zachar, Paul M Bingham, and Akiva Mintz, "Metabolic PET imaging in oncology." *American Journal of Roentgenology*, Vol. 209 (No. 2), pp. 270-76, (2017).
- 5- Sandip Basu, Habib Zaidi, Soren Holm, and Abass Alavi, "Quantitative techniques in PET-CT imaging." *Current Medical Imaging*, Vol. 7 (No. 3), pp. 216-33, (2011).
- 6- DW Townsend, "Physical principles and technology of clinical PET imaging." *Annals-Academy of Medicine Singapore*, Vol. 33 (No. 2), pp. 133-45, (2004).
- 7- Simon R Cherry *et al.*, "MicroPET: a high resolution PET scanner for imaging small animals." *IEEE Transactions on Nuclear Science*, Vol. 44 (No. 3), pp. 1161-66, (1997).
- 8- Hang-Keun Kim, Young-Don Son, Dae-Hyuk Kwon, Yohan Joo, and Zang-Hee Cho, "Wobbling and LSF-based maximum likelihood expectation maximization reconstruction for wobbling PET." *Radiation Physics and Chemistry*, Vol. 121pp. 1-9, (2016).
- 9- Zang-Hee Cho *et al.*, "Development of positron emission tomography with wobbling and zooming for high sensitivity and high-resolution molecular imaging." *IEEE Transactions on Medical Imaging*, Vol. 38 (No. 12), pp. 2875-82, (2019).
- 10- Peyman Sheikhzadeh, Hamid Sabet, Hossein Ghadiri, Parham Geramifar, Pardis Ghafarian, and Mohammad Reza Ay, "Design, optimization and performance evaluation of BM-PET: A simulation study." *Nuclear Instruments and Methods in Physics Research Section A: Accelerators, Spectrometers, Detectors and Associated Equipment*, Vol. 940pp. 274-82, (2019).
- 11- Azadeh Emami, Hossein Ghadiri, Pardis Ghafarian, Parham Geramifar, and Mohammad Reza Ay, "Performance evaluation of developed dedicated breast PET scanner and improvement of the spatial resolution by wobbling: a Monte Carlo study." *Japanese Journal of Radiology*, Vol. 38pp. 790-99, (2020).
- 12- A Chatziioannou, RW Silverman, K Meadors, TH Farquhar, and SR Cherry, "Techniques to improve the spatial sampling of microPET-A high resolution animal PET tomograph." *IEEE Transactions on Nuclear Science*, Vol. 47 (No. 2), pp. 422-27, (2000).
- 13- Joon Young Suk, "Improving the spatial resolution of the MicroPET R4 scanner by wobbling the bed." (2006).
- 14- Navid Zeraatkar *et al.*, "Development of a preclinical PET system based on pixelated LYSO crystals and SiPM arrays." in *2017 IEEE Nuclear Science Symposium and Medical Imaging Conference (NSS/MIC)*, (2017): IEEE, pp. 1-3.
- 15- S Pedemonte *et al.*, "GPU accelerated rotation-based emission tomography reconstruction." in *IEEE Nuclear Science Symposium & Medical Imaging Conference*, (2010): IEEE, pp. 2657-61.
- 16- Christof Knoess *et al.*, "Performance evaluation of the microPET R4 PET scanner for rodents." *European Journal of Nuclear Medicine and Molecular Imaging*, Vol. 30, pp. 737-47, (2003).
- 17- Mario Cañadas *et al.*, "Performance evaluation for 68 Ga and 18 F of the ARGUS small-animal PET scanner based on the NEMA NU-4 standard." in *IEEE Nuclear Science Symposium & Medical Imaging Conference*, (2010): IEEE, pp. 3454-57.
- 18- Jin Su Kim *et al.*, "Performance measurement of the microPET focus 120 scanner." *Journal of Nuclear Medicine*, Vol. 48 (No. 9), pp. 1527-35, (2007).
- 19- Andrew L Goertzen *et al.*, "NEMA NU 4-2008 comparison of preclinical PET imaging systems." *Journal of Nuclear Medicine*, Vol. 53 (No. 8), pp. 1300-09, (2012).
- 20- Rameshwar Prasad, Osman Ratib, and Habib Zaidi, "NEMA NU-04-based performance characteristics of the LabPET-8™ small animal PET scanner." *Physics in Medicine & Biology*, Vol. 56 (No. 20), p. 6649, (2011).
- 21- Marcin Balcerzyk *et al.*, "Initial performance evaluation of a high resolution Albira small animal positron emission tomography scanner with monolithic crystals and depth-of-interaction encoding from a user's perspective." *Measurement Science and Technology*, Vol. 20 (No. 10), p. 104011, (2009).
- 22- Luyao Wang *et al.*, "Performance evaluation of the TransPET® BioCaliburn® LH system: a large FOV small-animal PET system." *Physics in Medicine & Biology*, Vol. 60 (No. 1), p. 137, (2014).
- 23- Parisa Khateri, Werner Lusterhmann, Christian Ritzer, Charalampos Tsoumpas, and Günther Dissertori, "NEMA characterization of the SAFIR prototype PET insert." *EJNMMI Physics*, Vol. 9 (No. 1), pp. 1-15, (2022).